Journal Name

COMMUNICATION

Crystal structure, thermal expansion and electrical conductivity of $LaCo_xNi_yMo_zO_3$

Received 00th January 20xx,
Accepted 00th January 20xx

DOI: 10.1039/x0xx00000x

www.rsc.org/

V. Øygarden[a,†] and T. Grande[b]

The effect of Mo-substitution was investigated for the $LaCo_xNi_yMo_zO_3$ system, obtaining single-phase perovskite for Mo-substitutions up to 20 at%. The crystal structure of the perovskite changed from rhobohedral, orthorombic to monoclinic with increasing Mo-content. The thermal expansion was suppresed by Mo-substituion, while the electrical conductivity were also supresed but remained relatively high.

Introduction

Intermediate temperature solid oxide fuel cells (IT-SOFC) are receiving significant attention as the search for emission-free energy sources is becoming more pressing. The development of IT-SOFCs is limited due to a lack of effective and stable cathode materials operating at lower temperatures.[1] Efficient cathode materials must combine high electronic and ionic conductivity with high catalytic activity, as well as chemical and thermal stability.

$LaCoO_3$ and $LaNiO_3$ are perovskite materials, which have been extensively studied as potential cathode materials for SOFCs.[2-7] The solid solution series $LaCo_{1-x}Ni_xO_3$ has also received significant attention.[8-10] Although these materials demonstrate excellent electrical and catalytic properties, they suffer from the lack of chemical stability at elevated temperatures. Co-rich perovskites are also known to exhibit large, non-linear thermal expansion.[11] Recent reports have shown that B-site substitution of high valence cations, such as Nb^{5+}, can provide increased structural stability, whilst simultaneously lower the thermal expansion.[12, 13]

Here, we report on the effect of Mo-substitution for a system of $LaCo_xNi_yMo_zO_3$ perovskites. The compositions studied are presented in the pseudo-ternary phase diagram in Figure 1. The materials are labelled Mo(*x*) where *x* corresponds to the substitution level of Mo, meaning Mo0 is equivalent to $LaCo_{2/3}Ni_{1/3}O_3$ and Mo25 is equivalent to $LaNi_{0.75}Mo_{0.25}O_3$. The correlation between *x*, *y* and *z* can also be expressed as

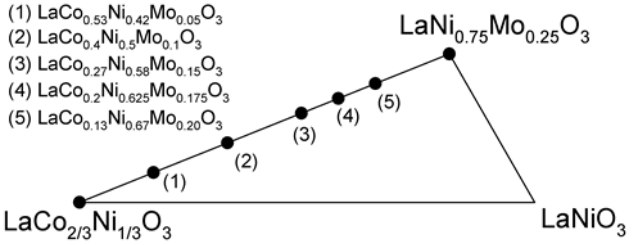

Fig. 1 Illustration of the compositions of the $LaCo_xNi_yMo_zO_3$ compositions in the pseudo ternary $LaCo_{2/3}Ni_{1/3}O_3$ – $LaNi_{0.75}Mo_{0.25}O_3$ – $LaNiO_3$ phase diagram.

$LaCo_{(2/3-8/3x)}Ni_{(5/3x+1/3)}Mo_xO_3$. Mo is assumed to be in a hexavalent oxidation state in these materials, which is a valid assumption when sintered in air. The stoichiometry of the compositions was chosen such to give a mixed oxidation state on the B-site, found as $Ni^{2+/3+}$, $Co^{2+/3+}$ or $Co^{3+/4+}$, depending on Mo-substitution.

Experimental

$LaCo_{(2/3-8/3x)}Ni_{(5/3x+1/3)}Mo_xO_3$ (x = 0, 0.05, 0.10, 0.15, 0.20 and 0.25) were prepared through a solid state synthesis route. Stoichiometric amounts of metal oxides (La_2O_3, Co_3O_4, NiO and MoO_3) were mixed in 100% ethanol and milled in a Retch PM100 planetary mill at 300 rpm for 20 min. Both crucible and grinding media (20 mm diameter spheres) were made from ZrO_2. La_2O_3 were dried at 700 °C for 6 h prior to use. The materials were then calcined at 1100 °C for 12 h and finally sintered at 1450 °C for 6 h.

Powder X-ray diffraction was performed using a Bruker AXS, D8 Focus equipped with a LynxEye detector and a Cu-radiation source. Data was collected in the 2θ-range 15 – 90°. Rietveld refinements were carried out using the Topas v4.2 software.[14]

[a] Department of Physics, Institute for Energy Technology, N-2007 Kjeller, Norway.
[b] Department of Materials Science and Engineering, Norwegian University of Science and Technology, N-7491 Trondheim, Norway.
† Corresponding author. E-mail: vegar.oygarden@ife.no

Diffraction patterns were fitted using a Thompson-Cox-Hastings pseudo-Voigt peak model and a Chebychev background model. A common thermal parameter was used for all the atoms in the unit cell.

Table 1. The average TEC from 100 – 700 °C, electrical conductivity at 700 °C, and lattice parameters obtained for $LaCo_{(2/3-8/3x)}Ni_{(5/3x+1/3)}Mo_xO_3$ (x = 0, 0.05, 0.10, 0.15, 0.20 and 0.25). R_{wp} describes the quality of the Rietveld refinements.

		Mo0	Mo5	Mo10	Mo15	Mo17.5	Mo20	Mo25
TEC (10^{-6} K^{-1})		17.0	20.6	18.0	16.4	13.8	13.0	-
σ (700 °C)		1168	493.3	155.0	28.7	22.0	41.1	10.7
Spacegroup		$R\bar{3}c$	$R\bar{3}c$	*Pbnm*	*Pbnm*	*Pbnm*	*Pbnm*	*P2₁/n*
a (Å)		5.4616(1)	5.4855(1)	5.5118(2)	5.5226(2)	5.5360(3)	5.5438(1)	5.5557(1)
b (Å)		5.4616(1)	5.4855(1)	5.4746(2)	5.5122(2)	5.5367(3)	5.5592(1)	5.5948(1)
c (Å)		13.1176(1)	13.1844(3)	7.7569(3)	7.8078(4)	7.8244(3)	7.8393(1)	7.8633(1)
β (°)		-	-	-	-	-	-	90.01
R_{wp} (%)		4.0	4.0	3.9	3.5	3.9	4.1	4.0
La	*x*	0	0	0.4963(8)	0.4916(5)	0.4896(4)	0.4903(4)	0.4863(3)
	y	0	0	0.5236(3)	0.5261(2)	0.5303(2)	0.5318(2)	0.5356(2)
	z	1/4	1/4	1/4	1/4	1/4	1/4	0.2493(4)
O1	*x*	0.439(1)	0.449(1)	0.531(6)	0.555(5)	0.554(4)	0.565(3)	0.545(4)
	y	0	0	0.999(3)	0.997(2)	0.998(2)	0.995(2)	0.991(2)
	z	1/4	1/4	1/4	1/4	1/4	1/4	0.251(2)
O2	*x*	-	-	0.190(6)	0.211(5)	0.249(3)	0.276(3)	0.233(5)
	y	-	-	0.759(3)	0.788(5)	0.826(2)	0.790(3)	0.782(5)
	z	-	-	0.022(3)	0.021(3)	0.016(2)	0.013(3)	1.012(4)
O3	*x*	-	-	-	-	-	-	0.186(4)
	y	-	-	-	-	-	-	0.279(5)
	z	-	-	-	-	-	-	1.012(4)

Thermal expansion was determined with a Netzsch DIL 402C dilatometer using 10 mm long cylindrical samples with 5 mm diameter. The instrument was calibrated using an alumina reference.

Electronic conductivity was measured using a four-point DC setup. Rectangular bars with dimensions of approximately 50 x 10 x 3 mm were used.

Results and Discussion

The X-ray diffraction patterns of the series of materials described in Figure 1 are presented in Figure 2. All materials were single-phase and assigned to a perovskite structure, with exception to Mo25 where a secondary phase of La_2MoO_6 was found in agreement with previous reports.[15] From the Rietveld refinement, the molar fraction of La_2MoO_6 was calculated to be ~3.2 mol%. The reflections in the diffraction pattern could be indexed to the $a^-a^-c^+$ tilt system for Mo10 – Mo25, which corresponds to both the monoclinic *P2₁/n* and the orthorhombic *Pbnm* space groups.[16] A significant intensity of the 011 reflection, indicating B-site ordering, could only be observed for Mo25. This allowed Mo25 to be assigned to the monoclinic space group while Mo10, Mo15, Mo17.5 and Mo20 were all indexed to the orthorhombic space group *Pbnm*. Mo0 and Mo5 were both indexed to the $a^-a^-a^-$ tilt system which correlates to the rhombohedral $R\bar{3}c$ space group. The unit cell parameters are summarized in Table 1.

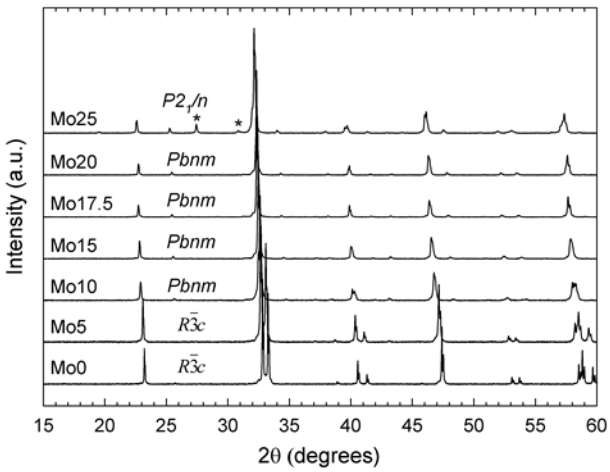

Fig. 2 X-Ray diffractograms of $LaCo_xNi_yMo_zO_3$. The numbers in the labels correspond to the Mo-fraction. (*) denote the diffraction peaks of La_2MoO_6.

The pseudocubic unit cell parameters and unit cell volume are presented as a function of Mo-content in Figure 3. The unit cell parameters increase with increasing Mo-content, which is expected from electroneutrality as the high valence of Mo reduces Ni and Co to lower oxidation states with higher ionic

radii. The unit cell volume exhibit a near-linear correlation with the Mo-content.

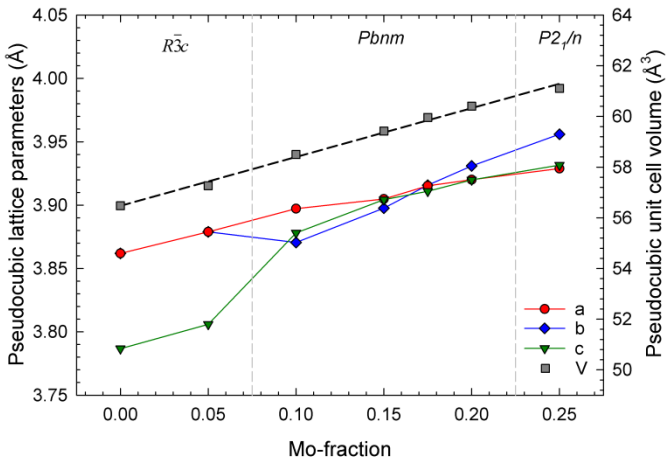

Fig. 3 The pseudocubic lattice parameters plotted as a function of Mo-content in $LaCo_xNi_yMo_zO_3$. The dotted line is a guide to the eye.

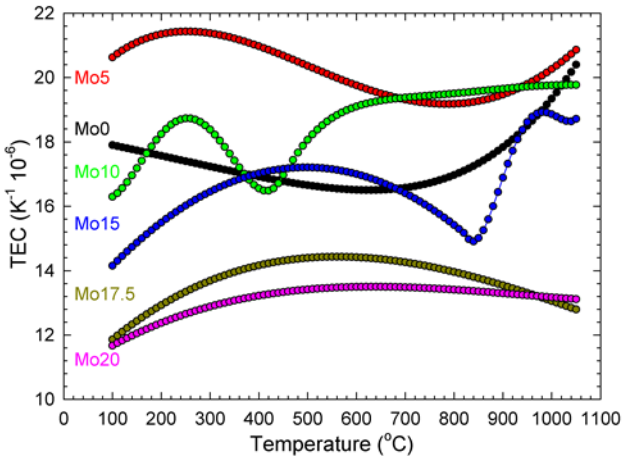

Fig. 4 Thermal expansion coefficient of the materials $LaCo_xNi_yMo_zO_3$. The numbers on the labels corresponds to the Mo-content.

The thermal expansion of the materials was measured in air, see Figure 4. No hysteresis was found when comparing the heating and cooling curves. The average TEC from 100 – 700 °C is given in Table 1. Interestingly, the thermal expansion coefficient (TEC) of Mo5 was higher than Mo0. The TEC decreased substantially with further Mo-substitution. A TEC maximum was seen for Mo5 at ~200 °C. Except Mo0, a TEC maximum was also found for the other materials, however, the extent of the maximum and the temperature of the maximum decreased with increasing Mo-content. Mo10 and Mo15 both exhibited a sharp TEC minimum, which could be rationalised by a first-order phase transition from orthorhombic to rhombohedral symmetry. A significant increase of the TEC was observed for Mo15 above the phase transition.

The TEC maxima observed are likely due to thermal population of higher spin-configurations of Co^{3+}.[4, 12] Based on extensive studies of the magnetic transitions in $LaCoO_3$, Co^{3+} is believed to exhibit three different spin-states: High-spin (HS) ($t_{2g}^4e_g^2$) (ionic radii = 0.64 Å), intermediate-spin (IS) ($t_{2g}^5e_g^1$) (ionic radii = 0.56 Å), and the low-spin (LS) ground state ($t_{2g}^6e_g^0$)

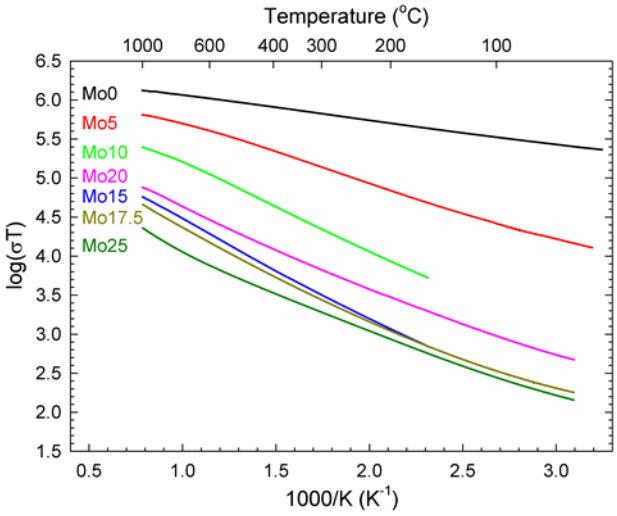

Fig. 5 log(σT) of the materials $LaCo_xNi_yMo_zO_3$ measured in air plotted as a function of reciprocal temperature.

(ionic radii = 0.545 Å).[2, 6, 17-21] Podlesnyak *et al.* [22] presented direct evidence by means of inelastic neutron scattering that the magnetic transition observed for $LaCoO_3$ at 40 K is a gradual population of HS states. Interactions between LS and HS states prevent HS states forming at nearest neighbour sites, causing the LS and HS states to order in an 1:1 ratio.[19] The equilibrium between the two spin states is upheld by a dynamic charge excitation reaction described as LS Co^{3+} ($t_{2g}^6e_g^0$) + HS Co^{3+} ($t_{2g}^4e_g^2$) → LS Co^{4+} ($t_{2g}^5e_g^0$) + HS Co^{2+} ($t_{2g}^5e_g^2$).[23] This is believed to be the cause of the increasing non-linear thermal expansion. At a critical temperature, the formation of IS states become energetically favourable according to the following reaction: LS Co^{4+} ($t_{2g}^5e_g^0$) + HS Co^{2+} ($t_{2g}^5e_g^2$) → 2 IS Co^{3+} ($t_{2g}^5e_g^1$). This reaction rapidly populates the IS states, thereby decreasing the average ionic radii of the B-site which is observed as a decrease of thermal expansion. These thermally induced spin-state transitions could explain the TEC maximums observed in Figure 4.

The DC electrical conductivity of the $LaCo_xNi_yMo_zO_3$ materials measured in air is presented in Figure 5. The absolute values at 700 °C are summarized in Table 1. All materials showed semiconducting behaviour, while both Mo0 and Mo5 exhibited a gradual transition to metallic conductivity at elevated temperatures. log(σT) is close to linear for Mo0 while the other materials in the series exhibit a slight enhancement of conductivity at intermediate temperatures. The conductivity decreased with increasing Mo-content with the exception of Mo20, which exhibited higher conductivity than both Mo15 and Mo17.5. Mo25 demonstrated the lowest conductivity in the series, however, the presence of the insulating secondary phase of La_2MoO_6 must be taken into account.

The decreasing conductivity with increasing Mo-content is expected since Mo^{6+} is a d^0-transition metal which decreases the density of states near the Fermi level. Acceptable electronic

conductivities are still present for relatively large Mo-substitutions, showing that sufficient conductivity is retained if the oxidation states of the host Co and Ni cations are optimised.

Attempts were made to substitute Sr for La in $LaCo_{0.2}Ni_{0.6}Mo_{0.2}O_3$ in order to introduce oxygen vacancies in the material to ensure good ionic conductivity. Only smaller levels of Sr-substitutions resulted in single-phase materials, while higher Sr-contents lead to multiphase materials containing three phases; a perovskite phase, $La_{1-x}Sr_xNiO_{4+\delta}$ and NiO. This can be rationalised by considering the stability of Ni^{3+} in perovskite materials at elevated temperatures in air. $LaNiO_3$ decomposes to the Ruddlesden-Popper material $La_4Ni_3O_{10}$ + NiO at ~980 °C in air, where the nominal oxidation state of Ni is +2.67.[24] At 1212 °C $La_4Ni_3O_{10}$ further decomposes to La_2NiO_4 + NiO with only Ni^{2+}. By large substitutions of La^{3+} with Sr^{2+} in $LaCo_xNi_yMo_zO_3$, the material compensates the extra charge by precipitating secondary phases with Ni^{2+} rather than accommodating large population of Ni^{3+}. The formation of significant concentrations of oxygen vacancies as a charge compensating mechanism appear to be stunted by the strong Mo-O bonds due to the hexavalent oxidation state of Mo.

Conclusions

Single phase materials in the $La_xNi_yMo_zO_3$ perovskite system were successfully prepared for Mo-substitutions up to 20 at%. Higher levels of substitutions resulted in multiphase materials. For lower Mo-contents (5 and 10 at% Mo) the crystal structure was assigned to a rhombohedral perovskite ($R\bar{3}c$), while the materials with Mo-content from 15 to 20 at% were assigned to an orthorhombic space group (*Pbnm*). The thermal expansion was significantly depressed with increasing Mo-substitution. The electronic conductivity also decreased with increasing Mo-content; however, significant conductivity was retained.

Acknowledgements

Financial support of the Research Council of Norway (RENERGY, grant no. 185322, Stack technology for ceramic proton conductors) is acknowledged.

References

1 A. Aguadero, L. Fawcett, S. Taub, R. Woolley, K. T. Wu, N. Xu, J. A. Kilner and S. J. Skinner, *J Mater Sci*, 2012, **47**, 3925-3948.
2 M. A. Korotin, S. Y. Ezhov, I. V. Solovyev, V. I. Anisimov, D. I. Khomskii and G. A. Sawatzky, *Phys. Rev. B*, 1996, **54**, 5309.
3 M. L. Medarde, *J. Phys.: Condens. Matter*, 1997, **9**, 1679.
4 P. M. Raccah and J. B. Goodenough, *Phys. Rev.*, 1967, **155**, 932.
5 K. P. Rajeev, G. V. Shivashankar and A. K. Raychaudhuri, *Solid State Commun.*, 1991, **79**, 591.
6 M. A. Senarisrodriguez and J. B. Goodenough, *J. Solid State Chem.*, 1995, **116**, 224.
7 X. Q. Xu, J. L. Peng, Z. Y. Li, H. L. Ju and R. L. Greene, *Phys. Rev. B*, 1993, **48**, 1112.
8 P. Hjalmarsson, M. Sogaard, A. Hagen and M. Mogensen, *Solid State Ionics*, 2008, **179**, 636.
9 P. Hjalmarsson, M. Sogaard and M. Mogensen, *J. Solid State Chem.*, 2010, **183**, 1853.
10 M. Hrovat, N. Katsarakis, K. Reichmann, S. Bernik, D. Kuscer and J. Holc, *Solid State Ionics*, 1996, **83**, 99.
11 F. M. Figueiredo, J. R. Frade and F. M. B. Marques, *Solid State Ionics*, 1999, **118**, 81.
12 V. Øygarden and T. Grande, *J. Solid State Chem.*, 2012, **192**, 246.
13 V. Øygarden and T. Grande, *Dalton Transactions*, 2013, **42**, 2704-2715.
14 BrukerAXS, *TOPAS V4*, 2008, Karlsruhe, Germany.
15 S. E. Hou, J. A. Alonso, S. Rajasekhara, M. J. Martinez-Lope, M. T. Fernandez-Diaz and J. B. Goodenough, *Chem. Mater.*, 2010, **22**, 1071-1079.
16 C. J. Howard, B. J. Kennedy and P. M. Woodward, *Acta Cryst.*, 2003, **B59**, 463.
17 K. Asai, A. Yoneda, O. Yokokura, J. M. Tranquada and G. Shirane, *J. Phys. Soc. Jpn.*, 1998, **67**, 290.
18 M. W. Haverkort, Z. Hu, J. C. Cezar, T. Burnus, H. Hartmann, M. Reuther, C. Zobel, T. Lorenz, A. Tanaka, N. B. Brookes, H. H. Hsieh, H. J. Lin, C. T. Chen and L. H. Tjeng, *Phys. Rev. Lett.*, 2006, **97**, 176405.
19 K. Knizek, Z. Jirak, J. Hejtmanek and P. Novak, *J. Phys. Condens. Matter*, 2006, **18**, 3285.
20 G. Maris, Y. Ren, V. Volotchaev, C. Zobel, T. Lorenz and T. T. M. Palstra, *Phys. Rev. B*, 2003, **67**, 224423.
21 P. G. Radaelli and S. W. Cheong, *Phys. Rev. B*, 2002, **66**, 094408.
22 A. Podlesnyak, S. Streule, J. Mesot, M. Medarde, E. Pomjakushina, K. Conder, A. Tanaka, M. W. Haverkort and D. I. Khomskii, *Phys. Rev. Lett.*, 2006, **97**, 247208.
23 Z. Jirak, J. Hejtmanek, K. Knizek and M. Veverka, *Physical Review B*, 2008, **78**, 014432.
24 M. Zinkevich and F. Aldinger, *J. Alloys Compd.*, 2004, **375**, 147.